9nm node wafer defect inspection using three-dimensional scanning, a 405nm diode laser, and a broadband source

Renjie Zhou[a,b,c], Chris Edwards[a,b], Casey A. Bryniaski[a], Gabriel Popescu[b], and Lynford L. Goddard*[a]

[a]Micro and Nanotechnology Laboratory, Department of Electrical and Computer Engineering
University of Illinois at Urbana-Champaign, Urbana, Illinois 61801, USA

[b]Quantitative Light Imaging Laboratory, Department of Electrical and Computer Engineering
Beckman Institute for Advanced Science and Technology
University of Illinois at Urbana-Champaign, Urbana, Illinois 61801, USA

[c]Currently with George R. Harrison Spectroscopy Laboratory, Massachusetts Institute of Technology, Cambridge, Massachusetts 02194, USA

ABSTRACT

We recently built a 405nm laser based optical interferometry system for 9nm node patterned wafer defect inspection. Defects with volumes smaller than 15nm by 90nm by 35nm have been detected. The success of defect detection relied on accurate mechanical scanning of the wafer and custom engineered image denoising post-processing. To further improve the detection sensitivity, we designed a higher precision XYZ scanning stage and replaced the laser source with an incoherent LED to remove the speckle noise. With these system modifications, we successfully detected both defects and surface contamination particles in bright-field imaging mode. Recently, we have upgraded this system for interferometric defect inspection.

Keywords: 9nm node wafer, wafer defect inspection, interferometric microscopy, laser defect inspection, white-light defect inspection

1. INTRODUCTION

The critical dimensions (CDs) in the semiconductor manufacturing process have been shrinking rapidly over the past decades. Integrated circuit (IC) devices based on the 14nm node process have been developed recently. At the same time, new architectures such as three-dimensional (3D) and monolayer based transistors are also being implemented into devices. Thus, detection of killer defects in a patterned silicon wafer has become a grand challenge [1, 2].

Currently, the most widely used wafer CD metrology tools are based on optical microscopy, scanning electron microscopy (SEM), and atomic force microcopy (AFM). A discussion on wafer critical dimension metrology is presented in reference [2]. Optical metrology methods are advantageous over other methods due to their nondestructive and high throughput nature. Most of the currently used optical metrology tools are based on scatterometry, ellipsometry, polarimetry, and interferometry. These techniques offer capabilities in wafer CD measurement, thin film characterization, mask inspection, and surface profiling capabilities. For the past several years, our group has developed a laser-based low-noise common-path interferometric inspection system, based on diffraction phase microscopy [3, 4], to detect wafer patterning defects in 32nm, 22nm node, and 9nm node wafers [5-8], and we have detected defects down to 20nm wide by 100nm long by 110nm tall.

In this paper, we present our recent results on improving the detection sensitivity for inspection of 9nm node densely patterned wafers. We first demonstrated a 405nm laser based interferometric microscopy system for defect inspection in this wafer. Using this system, defects smaller than 15nm by 90nm by 35nm have been detected and verified with SEM. The success of the defect detection was ensured by the common optical path interference geometry, wafer mechanical scanning, and image post-processing.

In order to detect even small defects, we investigated the wafer scanning stage and the light source. We first built a wafer

*lgoddard@illinois.edu; phone 1 217 244-0799; fax 1 217 244-6375; http://psl.mntl.illinois.edu

Metrology, Inspection, and Process Control for Microlithography XXIX, edited by Jason P. Cain, Martha I. Sanchez, Proc. of SPIE Vol. 9424, 942416 · © 2015 SPIE
CCC code: 0277-786X/15/$18 · doi: 10.1117/12.2085683

scanning stage with < 10nm stepping precision and improved repeatability. This wafer scanning stage is capable of performing scanning in x, y, and z. It is also equipment with tip/tilt and rotation correction. Then, we replaced our laser source with a broadband source. In contrast to lasers, broadband or incoherent light sources have low spatial and temporal coherence. The spatial coherence is determined by the spreading of the wavevector **k** in space, while the temporal coherence is determined by the spreading of the wavelength λ. Incoherent light imaging systems are speckle free due to their low coherence, thus allowing for highly sensitive measurements. We incorporated these modalities into a bright-field microscope for the 9nm node wafer defect inspection. We performed both transverse and vertical wafer scanning. By volumetric processing the scanning images, we successfully detected the intentionally fabricated defects. At the same time, our system can detect dust particles, sort them according to their size, and localize them in all three dimensions.

Interferometric measurement gives both the phase and amplitude information of the scattered field coming from the wafer. It allows us to obtain both the topography and the reflection information of the wafer structure. Thus, we added a common optical-path interferometer to the bright-field microscope system. The reference beam was achieved with a projector-based spatial light modulator (SLM). The signal beam can also be filtered spectroscopically with the SLM. We have verified the phase and amplitude measurement accuracy of our system by measuring reference samples.

2. 405 NM LASER INSPECTION SYSTEM SENSITIVITY TEST

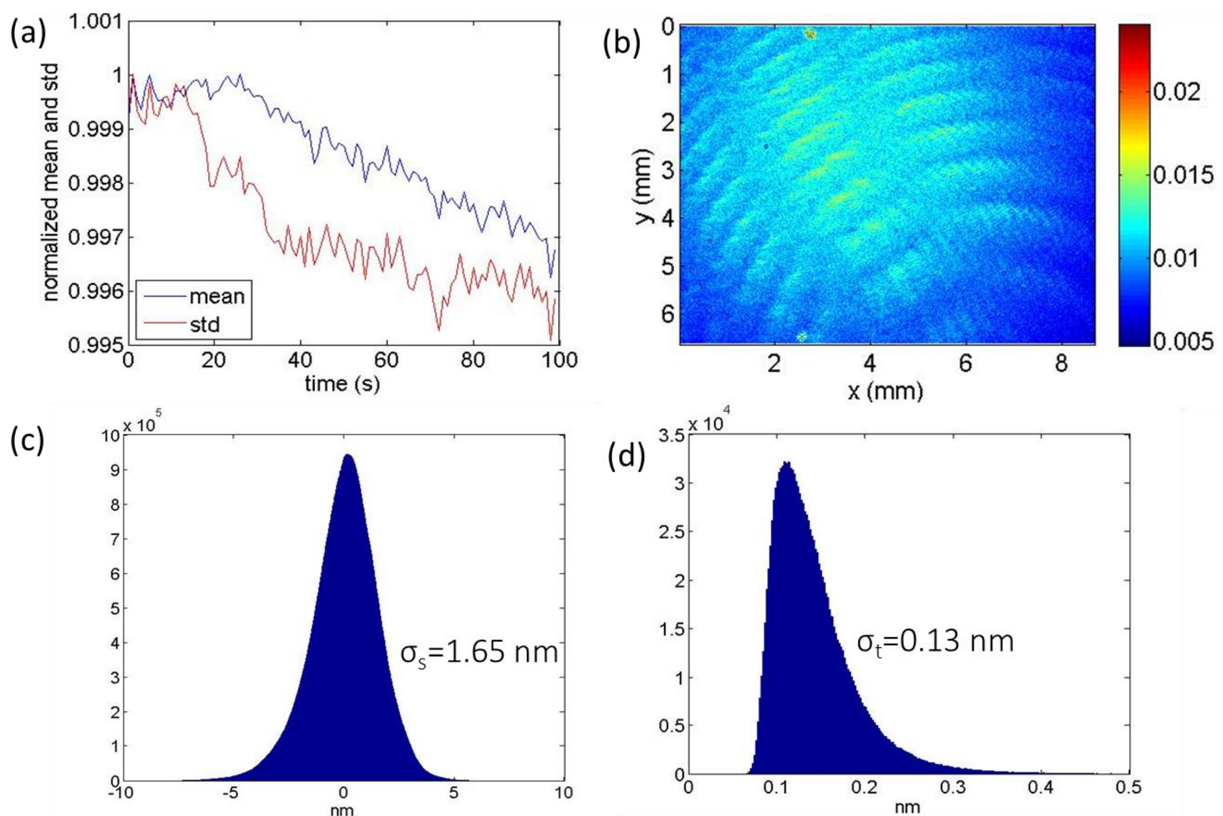

Figure 1. 405nm laser sensitivity characterization. (a) The intensity mean and standard deviation fluctuation over time. (b) The spatial distribution of the pixel intensity standard deviation over time. (c) The spatial noise histogram. (d) The temporal noise histogram.

In the past, we used a 532nm solid-state laser for the 22nm node wafer defect inspection. However, this laser has power instability issues which prevented us from detecting smaller defects on a 9nm node densely patterned wafer. Thus, we decided to use a more stable 405nm diode laser from QPhotonics (QFLD-405-20S). In Fig. 1(a)-(b), we test the laser source power stability by measuring the laser intensity distribution on a CCD camera over a 100s time period. We calculate the mean and the standard deviation of the intensity at each frame and plot them as a function of time as shown

in Fig. 1(a). From this figure, we see that the mean and the standard deviation fluctuates less than 0.5%, which is an order of magnitude improvement over our previous 532nm laser. At each pixel, we also calculate its standard deviation in time over the image acquisition period. The spatial distribution of the pixel power deviation is plotted in Fig. 1(b), where we achieved less than 1.5% standard deviation everywhere. This means that the laser source is stable both in time and space. After the laser power stability test, we incorporated the laser into our interferometry imaging system. To further improve the laser power stability in the imaging system, we added a Faraday rotator based isolator after the laser to prevent back reflection of the light into the laser cavity. In addition, we inserted a 405 nm narrow-band filter in front of the camera to remove the ambient room light. We characterized the system sensitivity by measuring a flat sample and retried its phase and amplitude with 256 frames at two different fields of view. The spatial noise histogram and the temporal noise histogram are plotted in Fig. 1(c) and (d), respectively. The spatial noise is determined to be 1.65nm and the temporal noise is determined to be 0.13nm by using the FWHM width of the histograms. Compared with the 532nm laser system, the spatial noise has been reduced by more than 3x and the temporal noise has been reduced by more than 6.5x.

3. 9NM NODE WAFER INSPECTION RESULTS WITH THE 405NM LASER

In the 405nm laser interferometry inspection system, we scanned the 9nm node wafer horizontally and collected an image stack (see more detail of this system configuration and the image post-processing in reference [7]). From the image stack, we retrieved the phase and amplitude images and used them to produce the 2nd difference images. In Fig. 2 (a), we stitched the 2nd difference phase image and produce a panoramic image, where we observe the defect tripole pattern indicated by a red rectangle. To extract the tripole pattern, we convolved the panoramic image with a matched tripole pattern and show the result in Fig. 2(b). The same processing is performed on the 2nd difference amplitude images; see Fig. 2(c) for the panoramic phase image and Fig. 2(d) for this image after a matched tripole convolution. In Fig. 3, we show the SEM verification for this detected defect. In the zoomed-in image in Fig. 3(b), the defect is marked with a red rectangle.

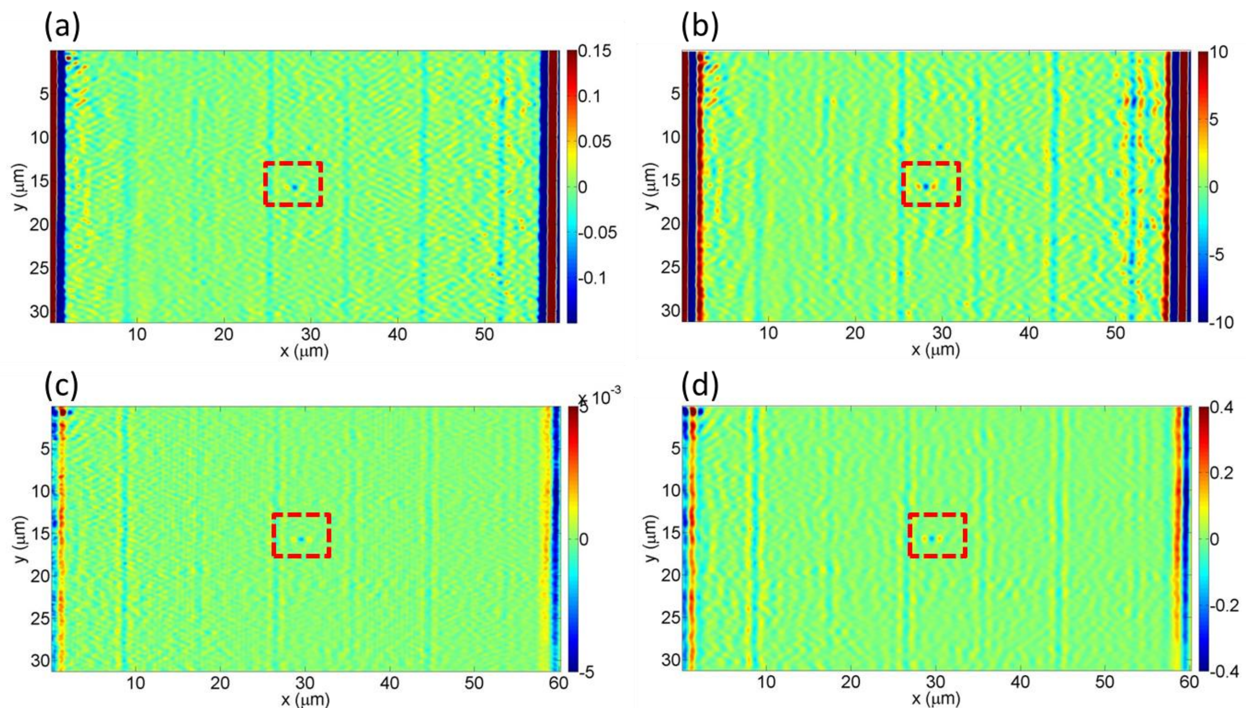

Figure 2. The processed phase and amplitude images using the 405nm laser inspection system. (a) The panoramic 2nd order difference phase image. (b) The image after convolution with the tripole pattern. (c) The panoramic 2nd order difference amplitude image. (b) The image after convolution with the tripole pattern. The defect is marked by a red rectangle.

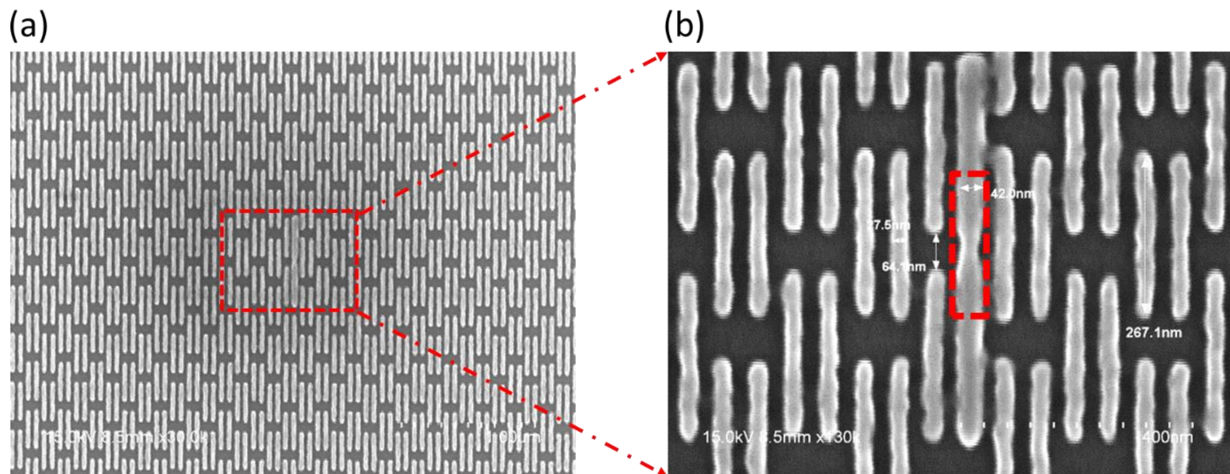

Figure 3. SEM images in a parallel bridge array. (a) SEM image with the defect in the center enclosed by a red box. (b) A zoomed-in SEM image of the defect. The defect is marked by a red rectangle.

4. BROADBAND BRIGHT-FIELD DEFECT INSPECTION

In Fig. 4, we illustrate the white-light bright-field inspection system. This system is equipped with a high precision XYZ (3D) sample scanning stage that we have recently built to move the sample across the field of view and through the focus. We used a white-light LED as the broadband light source which was first imaged onto the aperture diaphragm. The diaphragm selects the portion of the filament source for Köhler illumination. The back focal plane of the objective is the conjugate plane of the aperture diaphragm. Thus, plane waves at different angles illuminate the sample, ensuring uniform intensity on the sample.

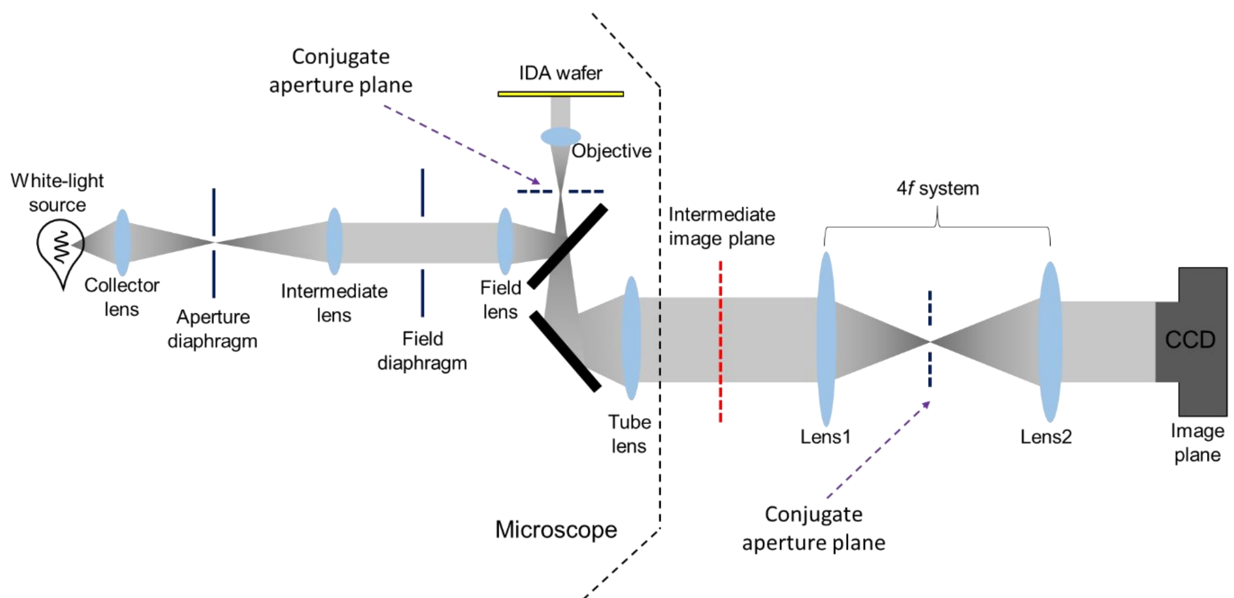

Figure 4. The Köhler-illumination white-light bright-field microscopy system.

In white-light bright-field imaging, the spatial coherence of the light source is an important factor to consider, especially for improving the image contrast in the context of the modulation transfer function [9], which is crucial for quantitative

measurements of the surface profile in interferometry [10] (this reference is a complete study of spatial coherence for white-light interferometry with a transmission white-light DPM system as an example). By adjusting the condenser aperture size, the spatial coherence length l_s of the light source on the sample can be also controlled, described by the relation $l_s=0.61\lambda/NA_{con}$, where NA_{con} is the condenser numerical aperture at the back focal plane of the objective. To achieve the best contrast, l_s needs to be sufficiently large such that the illumination on the sample field of view acts like a plane wave. This is important for phase imaging, which we will discuss in the following section. The temporal coherence is another important factor to consider that relates to the image contrast with speckle. The temporal coherence length is inverse proportional to the spectral bandwidth. A smaller temporal coherence length illumination suffers less speckle noise. The spatial coherence also affect the speckle and this was confirmed with a super-continuum light source [10] (with small temporal coherence length and large spatial coherence length, but has speckle like a regular laser). The 4*f* system after the intermediate image plane is used to relay and magnify the sample pattern onto the camera plane.

Here, we used this system to inspect the 9nm node wafer which has contamination particles in addition to the central intentional defect. We scanned the wafer in the z-direction, i.e. through focus, with a 50nm step size over a 10μm range at 3 different locations spaced 1μm apart in the x-direction. Thus, a 2nd difference volume image is produced. Figure 5(a) is an xy plane image at the best focus. The dust particles and the intentional defect are both in focus in this plane. To improve the defect and particle signal contrast, we look at the particles and the defect, which are labeled by the numbers on the bottom, in the yz cross-sectional plane (cut along x-axis) images. Note that each yz plane image is individually normalized. Label 5 is the intentional defect, while the other labels are the dust particles. In the corresponding cross-sectional plane images, we can localize the particles in all dimensions by fitting their intensity distributions with three-dimensional Gaussian profiles.

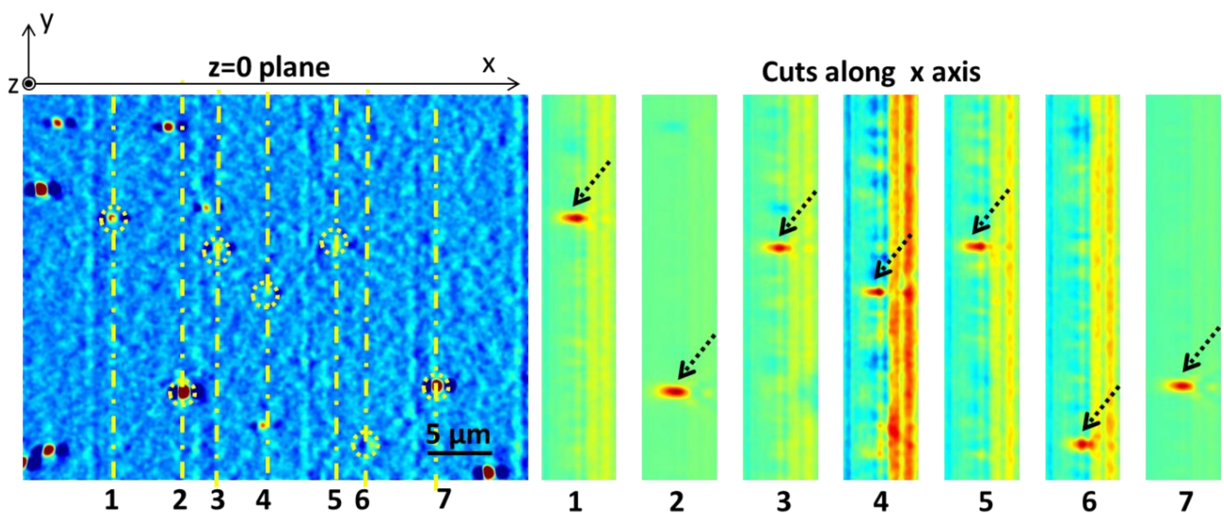

Figure 5. Defect inspection with the LED light source. The cross-sectional images for the dust particles and the defect labeled with the numbers are plotted.

5. BROADBAND INTERFEROMETER DESIGN

To make an interferometer, we need to create a reference beam and a signal beam. This was done with a diffraction grating and a projector based spatial light modulator (SLM), as shown in Fig. 6. We used a 110 lpm grating at the intermediate image plane which creates multiple orders of the image. And in the Fourier plane of the 4*f* system, the SLM passes the +1st diffraction order and low-passes the 0th diffraction order by projecting a black (block) and white (transmission) pattern from a PowerPoint slide on a laptop. Notice that, to avoid creating astigmatism for the image in the laser interferometric system, we low-pass the +1st diffraction order and let the 0th diffraction order be the image order, which always passes through the center of the lens. However, in broadband interferometry system the +1st order would spread out all the colors in the SLM plane due to dispersion, making it impossible to low-pass filter it. Thus, the broadband interferometry system uses the 1st order as the image order and suffers from astigmatism. After building the

interferometer, we verified the system performance by measuring the surface profile and the reflection images of test structures. Currently, we are working on implementing this system for 9nm node wafer defect inspection.

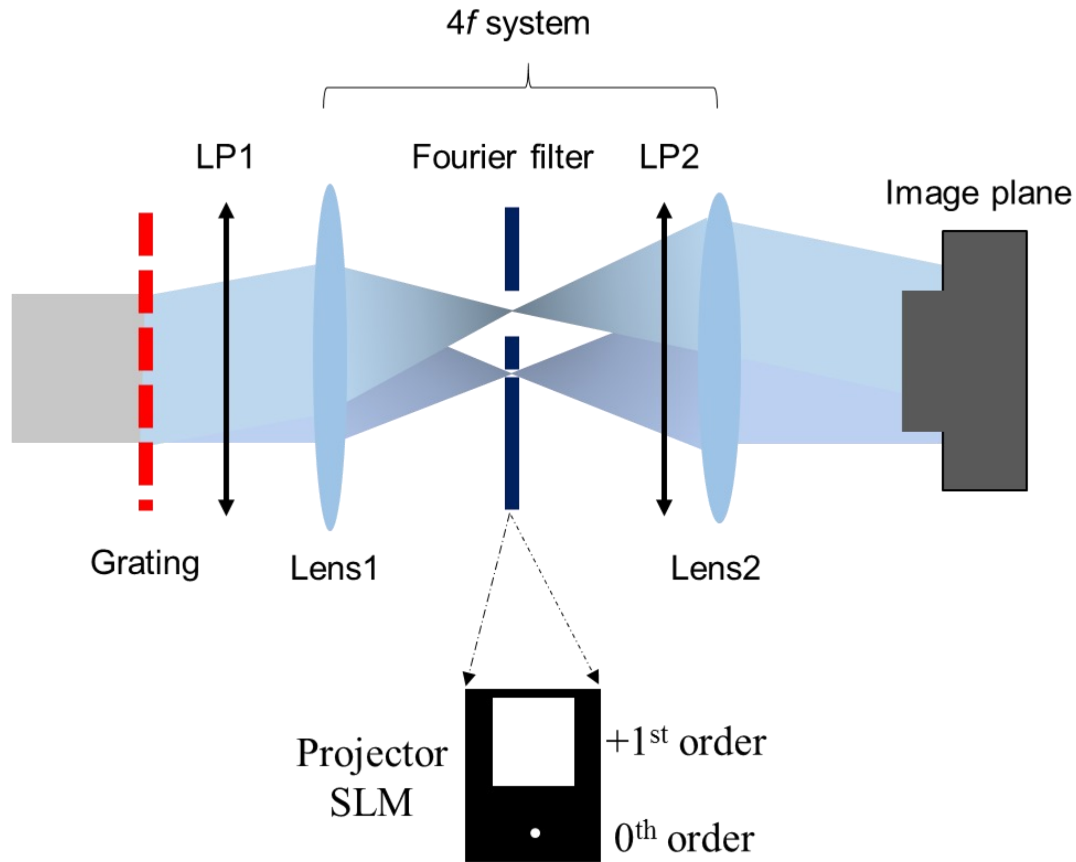

Figure 6. The interferometer system for the broadband interferometry inspection system.

6. CONCLUSION

The current progress on 9nm node wafer defect inspection has been presented. By using our highly stable 405nm laser interferometry system, defects down to 15nm by 90nm by 35nm has been detected and verified. The detection sensitivity of our system depends on mechanical scanning precision and light source stability and its coherence. By using an XYZ wafer stage with <10 nm step size and a stable white-light source, we significantly improved our system sensitivity. In the future, we will implement our white-light defect inspection system for detecting defects in 9nm node or even smaller design nodes densely patterned wafers.

ACKNOWLEDGMENTS

This research was supported by Semiconductor Research Corporation (contract P13117) and by the National Science Foundation (grant CBET-1040462 MRI) with matching funds from the University of Illinois. SEMATECH provided the test wafers. RZ was also supported by the Arnold and Mabel Beckman Foundation through its graduate fellowship program.

REFERENCES

[1] Crimmins, T. F., "Defect metrology challenges at the 11-nm node and beyond," Proc. SPIE **7638**, 76380H (2010).

[2] Foucher, J., Ernst, T., Pargon, E. and Martin, M., "Critical dimension metrology: perspectives and future trends," SPIE Newsroom (2008).
[3] Popescu, G., Ikeda, T., Dasari, R. R. and Feld, M. S., "Diffraction phase microscopy for quantifying cell structure and dynamics," Opt Lett **31**, 775-777 (2006).
[4] Edwards, C., Arbabi, A., Popescu, G., and Goddard, L. L., "Optically monitoring and controlling nanoscale topography during semiconductor etching," Light Sci Appl **1**, e30 (2012).
[5] Zhou, R., Edwards, C., Popescu, G. and Goddard, L. L., "Diffraction phase microscopy for wafer inspection," in *Photonics Conference (IPC), 2012 IEEE*(2012), pp. 644-645.
[6] Zhou, R., Popescu, G. and Goddard, L. L., "22 nm node wafer inspection using diffraction phase microscopy and image post-processing," SPIE **8681**, 86810G (2013).
[7] Zhou, R., Edwards, C., Arbabi, A., Popescu, G., and Goddard, L. L., "Detecting 20 nm wide defects in large area nanopatterns using optical interferometric microscopy," Nano Lett **13**, 3716-3721 (2013).
[8] Zhou, R., Edwards, C., Popescu, G. and Goddard, L. L., "9nm node wafer defect inspection using visible light," Proc. SPIE **9050**, 905017 (2014).
[9] Goodman, J. W., *Introduction to Fourier Optics* (Roberts & Co., 2005).
[10] Edwards, C., Bhaduri, B., Nguyen, T., Griffin, B., Pham, H., Kim, T., Popescu, G. and Goddard, L. L., "The effects of spatial coherence in diffraction phase microscopy," Opt. Exp. **22**, 5133-5146 (2014).